Journal of Theoretical and Applied Physics (2020) 14:181–194
https://doi.org/10.1007/s40094-020-00376-3

RESEARCH

One-dimensional simulation of hydrogen production kinetic models by water vapor plasmolysis in a DBD plate reactor

Mostafa El-Shafie[1] · **Shinji Kambara**[1] · **Yukio Hayakawa**[1]

Received: 23 December 2019 / Accepted: 22 April 2020 / Published online: 2 May 2020

Abstract

The results of one-dimensional time-dependent simulation modeling of hydrogen production from water vapor dissociation using non-thermal discharge plasma in a plate-type reactor were developed. Three different water vapor dissociation reaction mechanisms pathway models were simulated at a water vapor temperature of 573 K and same boundary conditions. The electron collision cross sections of electron water vapor were utilized based on the reaction mechanisms. The electron attachment and detachment processes were described in detail; additionally, the surface charge accumulation, recombination of charged species, positive and negative ions production and losses are considered. The electron density, electric field, electric potential, electron temperature and the hydrogen mass fraction are presented across the plasma discharge gap and over time. The first model was described as direct water vapor decomposition into their constituent's elements hydrogen and oxygen molecules. It was revealed that the formed hydrogen molecules increased across the plasma discharge gap over time. In model II, the simulation reaction mechanisms pathway included products of H_2O^+, OH^+, and O^+ ions. It was found a significant change in the electric potential and electric field across the discharge gap due to the charged species inside the plasma gap. In model III, it was introduced H^- radicals which controlled H atoms production by the electron detachment reaction. The most interesting results of these simulation models were the growing of hydrogen molecules across the plasma gap over time. Further, it was observed that the produced hydrogen mass fraction from model III was higher than model II and model I.

Keywords DBD simulation · Hydrogen production · Plate-type reactor · Electron density

Introduction

Hydrogen fuel offers many advantages such as lower emissions of greenhouse gases (GHGs) which could be utilized as alternative fuel. Hydrogen fuel can be produced by different methods using a renewable energy sources [1–5]. Steam methane reforming process acts 80–85% of the total world hydrogen production. All of hydrogen production technologies are directly or indirectly utilized fossil fuel; subsequently, GHGs emit to the environment. One-dimensional heat diffusion equation has been developed to find solution for the heat transfer problems [6, 7]. The results have been shown accuracy for the analytical solution. Moreover, a new integral solution has been developed for solving the heat and diffusion equations [8, 9]. The current work simulates and analyzes one-dimensional model of the hydrogen production from water vapor using dielectric barrier discharge plasma (DBD) which is cleaner than the hydrogen production from the conventional methods.

Studying of plasma and species characteristics has more attention due to their successful experimental results and applications at atmospheric pressure such as engineering, sterilization and surface treatment [10–15]. DBD plasma is considered the most important plasma type due to their high efficiency, productivity of new radicals, easy setup and operation. Hydrogen production from water vapor using plasma has recently more interest because of the high specific productivity [16]. DBD Plasma can be generated from electrical energy between two electrodes separated by dielectric quartz glass; it will transform it to kinetic electrons energy which transformed into new molecular kinetic energy of heavy particles [17].

✉ Mostafa El-Shafie
mostafaelshafie81@gmail.com

[1] Environmental and Renewable Energy Systems Division, Graduate School of Engineering, Gifu University, 1-1 Yanagido, Gifu 501-1193, Japan

Water is considered the third most important abundant molecule in the world after hydrogen and carbon monoxide gases [18]. Because of the continuous increase in global temperature, more water vapor will be evaporated and holding by the atmosphere. Hence, it was clear that it has an implication on the warming effect. Additionally, it can be considered an important greenhouse gas and also, contributing more than half of 33 K of natural warming [19]. Further, water is one of the dominant components of the biological cells and furthermore, water is the main of hydrocarbon fuels combustion products. Due to the importance of water stated above, electron collisions are stated to play an important role to determine the population of water molecules using plasma technique [20]. The water vapor electron collisions have been studied by many researchers for many years and reporting the cross section data for many interactions [21–25]. All water vapor collision processes including the total scattering, elastic scattering, momentum transfer, excitation of rotational, vibrational, and electronic states, ionization, electron attachment, dissociation, and emission of radiation have been reviewed by Y. Itikawa and N. Mason [26]. The electron collision cross sections are important inputs data to executing simulation. Many simulation studies for atmospheric DBD plasma have been carried out such as modeled of co-axial reactor in pure helium [27–30]. Most of plasma studies have been carried out and reported at low pressure [31–36].

In this study, three models were simulated for water vapor plasmolysis at atmospheric pressure in the plate-type reactor. These models are gradually complicated in their chemical reaction mechanisms pathway from model I to model III. The first model was analyzed for the direct water vapor decomposition reaction mechanism pathway. Model II and model III are more complicated included different ions. The electron collision cross sections for all models are prepared and utilized. In this simulation study, the electron density, electric field, electric potential, electron temperature and the hydrogen mass fraction are analyzed across the discharge gap and over time. Comparison between the hydrogen mass fractions of these models over the time across the discharge gap was investigated.

Water molecular properties

Water molecule can be found in the electronically ground state; additionally, water has a permanent of electric dipole moment which appears in its direction as shown in Fig. 1. The ionization energy of H_2O has been investigated as follows [37]:

$E_i = 12.621(\pm 0.002)$ eV

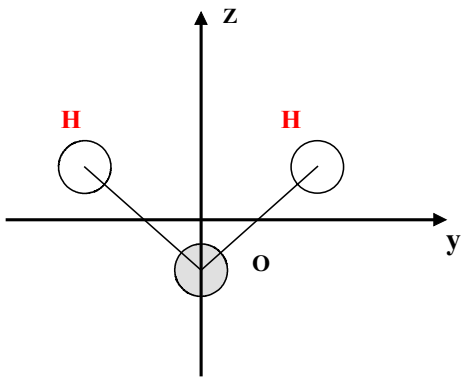

Fig. 1 Nuclear configuration of H_2O

A critical assessment and a very extensive analysis have been implemented to determine the dissociation energy of the water molecules to be [38],

$D(\mathrm{H-OH}) = 5.0992(\pm 0.0030)$ eV

Several reviews have been executed for electron collisions with water. The water vapor dissociation cross sections data have been prepared from the published collision cross sections pervious work [26, 45].

Simulation models kinetics

In recent years, many researchers' efforts have been carried out for modeling the water vapor decomposition using plasma. Electronic and ionic collisions with the water vapor for a single-type plasma-chemical reaction to overall kinetic models have been investigated [13, 17, 35, 39]. A mathematical model for the water chemical reactions inside the discharge channel has been proposed by Mededovic and Loke [34]. The discharge channel is divided into the core and recombination zones; the molecular hydrogen evolution has been described. The water vapor molecule at very low pressure (133-150P1), zero dimensional models has been studied [35]. They found that the major positive and negative species were H_3O^+ and OH^-, respectively. Vibrational excitation and dissociative electron attachment of the water vapor plasmolysis mechanism have been discussed [26]. The distribution of electron energy through different pathways in water vapor plasma is shown in Fig. 2. It can be observed that 80% of energy is absorbed by the vibrational excitation channel at low electron energy levels lower than 1 eV, while the most of energy is absorbed in the dissociative attachment reaction type at typical plasma electron temperatures levels of 3–5 eV [40]. The recommended ionization energy of H_2O is determined as follows [41]: $E_i = 12.62(\pm 0.002)eV$.

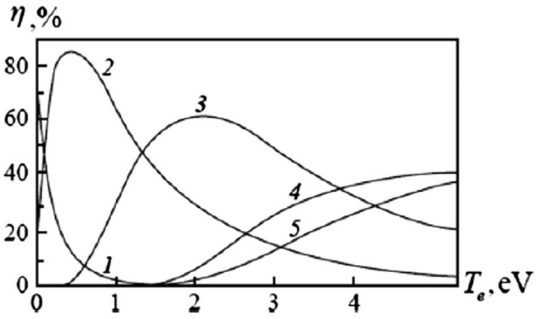

Fig. 2 Electron energy distribution between excitation dissociation and ionization channels in water vapor. (1) Elastic scattering; (2) vibrational excitation; (3) dissociative attachment; (4) electron excitation; (5) Ionization (Ref. [42])

Geometry

In this paper, the water vapor decomposition using DBD plasma in a plate-type reactor was simulated. Three models with different reaction mechanisms of water vapor plasmolysis were simulated using the water vapor cross section of electron collisions. The DBD plasma was driven by a sinusoidal typical power with high voltage source of 18 kV and frequency of 10 kHz. The electron density assumed to be 10^6 m^{-3}, the vapor pressure 1.01×10^5 Pa and temperature of 573 K. The cross sections of electron collisions of water vapor were obtained from the published cross section data. The selection criteria of the cross sections data were concluded as follows: the priority for experimental methods and the reliability of the experimental methods [26]. The plasma discharge gap is 4.5 mm. The thicknesses of the dielectric glass and mesh parts are 2 mm and 0.3 mm, respectively.

DBD Modeling equations

In this simulation, the DBD fluid dynamics equations were used. The surface chemistry reactions were considered for different species to calculate the production rate and the electrode surface losses [43]. The simulation models are implemented using COMSOL Multiphysics package [44]. The electron density and the electron mean energy were determined by solving a pair of drift diffusion equations. The convection of electrons due to fluid motion in these calculations is neglected. The simulation modeling equations are

$$\frac{\partial n_e}{\partial t} + \nabla \cdot \vec{\Gamma}_e = R_e - (\vec{u} \cdot \nabla) n_e \tag{1}$$

$$\vec{\Gamma}_e = -\left(\overrightarrow{\mu_e} \cdot \vec{E}\right) n_e - \overrightarrow{D_e} . \nabla n_e \tag{2}$$

where n_e is the electron density, the electron diffusion coefficient D_e, $\vec{\Gamma}_e$ is the electron flux, $\vec{u}$ is the average fluid velocity, and R_e is the rate of electron production.

The electron flux is caused by the electric field and by the density gradient. The electron energy density equation can be expressed as follows:

$$\frac{\partial n_\varepsilon}{\partial t} + \nabla \cdot \vec{\Gamma}_\varepsilon \left[-n_\varepsilon \left(\overrightarrow{\mu_\varepsilon} \cdot \vec{E} \right) - \overrightarrow{D_\varepsilon} \cdot \nabla n_\varepsilon \right] + \vec{E} \cdot \vec{\Gamma}_\varepsilon = R_\varepsilon - (\vec{u} \cdot \nabla) n_\varepsilon \tag{3}$$

$$\vec{\Gamma}_\varepsilon = -n_\varepsilon \left(\overrightarrow{\mu_\varepsilon} \cdot \vec{E} \right) - \overrightarrow{D_\varepsilon} \cdot \nabla n_\varepsilon \tag{4}$$

The amount of energy gained from the electric field by the electron indicates in this term $\vec{E} \cdot \vec{\Gamma}_\varepsilon$. The energy rate from the inelastic collisions can be estimated by:

$$R_\varepsilon = S_{en} + \frac{Q + Q_{gen}}{q} \tag{5}$$

where S_{en} indicates the power dissipation, Q_{gen} is the main heat source, and q is the electron charge. The electron diffusion coefficient D_e, the energy mobility μ_e, and the energy diffusion coefficient can be determined by:

$$D_\varepsilon = \mu_\varepsilon T_e, D_e = \mu_e T_e, \mu_\varepsilon = \frac{5}{3} \mu_e \tag{6}$$

While the electron energy source R_e and the energy loss due to inelastic collision R_ε can be given by:

$$R_e = \sum_{j=1}^{M} x_j k_j N_n n_e \tag{7}$$

where x_j is the mole fraction of the target species reaction j, k_j is the reaction rate coefficient (m^3/s), and the total neutral number of density is N_n ($1/m^3$). The electron energy loss is determined by summing all reactions collisional energy loss as follows:

$$R_\varepsilon = \sum_{j=1}^{P} x_j k_j N_n n_e \Delta\varepsilon_j \tag{8}$$

The energy loss from the reaction j is $\Delta\varepsilon_j$ (V); it can be computed from the reactions cross section data as follows:

$$k_k = \gamma \int_0^\infty \varepsilon \sigma_k(\varepsilon) f(\varepsilon) \mathrm{d}\varepsilon \tag{9}$$

where $\gamma = (2q/m_e)^{1/2} \left[C^{1/2}/kg^{1/2} \right]$, where q is the electron charge, and m_e is the electron mass [kg], ε is the energy [V], σ_k is the collision cross section [m^2] and will be explained for each model, and f is the electron energy distribution function. In non-electron species, the following equation is solved from the mass fraction for each species:

$$\rho\frac{\partial w_k}{\partial t}+\rho\left(\vec{u}\cdot\nabla\right)w_k=\nabla\cdot\vec{j_k}+R_k \tag{10}$$

where w_k is the density of ions, and $\nabla\cdot\vec{j_k}$ is the ions energy flux. The electrostatic field can be determined from the following equation:

$$-\nabla\cdot(\varepsilon_0\varepsilon_r E)=\rho \tag{11}$$

where ε_0 is the permittivity of vacuum, and ε_r is the relative dielectric constant. Due to the DBD plasma random motion effect of resulted electrons, the boundary conditions of the electron flux and electron energy flux can be estimated as follows:

$$n\cdot\vec{\Gamma}_e=\left(\frac{1}{2}v_{e,th}n_e\right)-\sum_p\gamma_p\left(\overrightarrow{\Gamma_p}\cdot n\right) \tag{12}$$

$$n\cdot\vec{\Gamma}_\varepsilon=\left(\frac{5}{6}v_{e,th}n_\varepsilon\right)-\sum_p\varepsilon_p\gamma_p\left(\overrightarrow{\Gamma_p}\cdot n\right) \tag{13}$$

In Eq. (12), the term on the right side is the produced electrons due to the secondary emission effect, where the secondary emission coefficient is γ_p. The secondary emission of energy flux is indicated in Eq. (13); ε_p is the mean energy of the secondary electrons.

In this DBD plasma simulation, the high voltage discharge electrode is driven by a sinusoidal electric potential and applied for the mesh electrode part,

$$V=V_0\sin(wt)\,[\mathrm{V}] \tag{14}$$

where V_0 is the applied peak voltage ($V_0=750$ V), and w is the angular frequency, while the DBD applied frequency is 10 kHz. Furthermore, the ground electrode is connected to the bottom plate as shown in Fig. 3.

Reaction mechanism and cross section of Model I

In this model, a direct water decomposition reaction mechanisms are used; the reaction mechanism of model I is shown in Table 1.

In this model, a direct and simple water vapor dissociation reaction mechanisms are investigated [45]; the gross and partial ionization cross section for electrons in the energy range of 0.1–20 keV have been used as shown in Table 2. It can be determined from the following relation

$$\sigma=\left(\frac{I^+}{I^-}\right)(\iota_p)^{-1}\left[T/\left(273\times3.535\times10^{16}\right)\right]\mathrm{cm}^2 \tag{15}$$

where I^+ is the current of positive ions to the measuring electrode; I^- is the electron current to the Faraday cage; l is the length from which ions are extracted in centimeters; p is the gas pressure in Torricelli; and T is the gas temperature in degrees Kelvin (room temperature). This is the first

Table 1 Ionization cross section for electrons on H_2O gas [45]

Reaction	Reaction type	Type
1	$H_2O+e\rightarrow H_2O+e$	Momentum transfer reaction
2	$H_2O+e\rightarrow H_2+1/2O_2$	Dissociation reaction

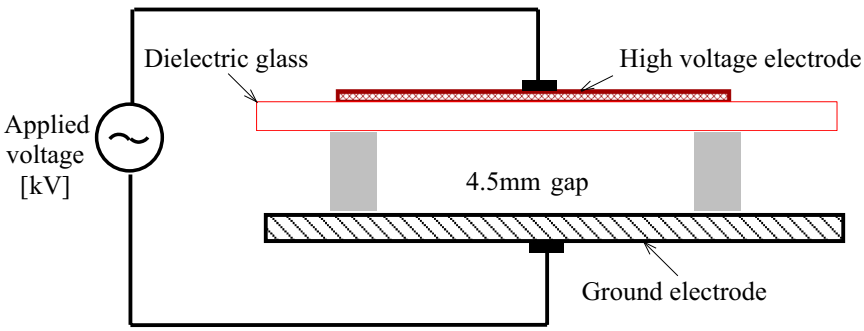

(a) Illustration of the MPR typical DBD plasma.

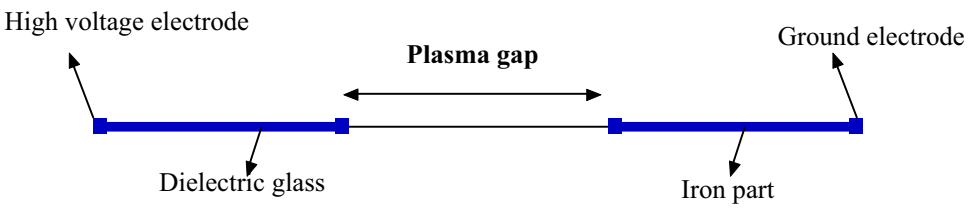

(b) 1-D simulated geometry.

Fig. 3 **a** Illustration of the MPR typical DBD plasma. **b** 1-D simulated geometry

Table 2 Ionization cross section for electrons on H_2O gas [45]

Energy [keV]	$\sigma H_2O \times 10^{-16}$ [cm^2/molecule]	$\sigma H_2 + 1/2O_2 \times 10^{-16}$ [cm^2/molecule]
0.08	1.98	…
0.09	2.01	…
0.1	1.98	2.1
0.12	1.96	2.05
0.16	1.83	1.89
0.2	1.71	1.75
0.3	1.46	1.34
0.4	1.26	1.22
0.5	1.12	1.06
0.6	1	0.94
0.8	0.77	0.75
1	0.622	0.649
2	0.375	0.374
3	0.261	0.271
4	0.22	0.214
5	0.183	0.182
6	0.16	0.153
8	0.123	0.121
10	0.101	0.101
12	0.088	0.086
14	0.078	0.076
16	0.064	0.069
18	0.058	0.062
20	0.054	0.058

successful trail of water vapor decomposition simulation using DBD plasma. Firstly, to simplify the water plasmolysis simulation, we started using the direct water vapor decomposition reaction mechanism with the following cross section.

Reaction mechanism and cross section of Model II

In this model, the simulation was carried out for more complicated water plasmolysis reaction mechanism. The electron collisions of H_2O molecules are excited to these levels: rotational, vibrational and electronic levels [26]. Some of water vapor plasma reactions may occur but aren't considered in this simulation study due to its high energy requirement and low probability [39],

$$H_2O + e \rightarrow 2H + O^+ + 2e$$
$$H_2O + e \rightarrow H^+ + O + H + 2e$$
$$H_2O + e \rightarrow 2H + O + e$$

The formation of produced radicals like hydrogen-H, hydroxyl-OH and oxygen-O in the non-thermal plasma is considered the most important process. After that these species react with each other to form new molecular products [34, 46, 47]. Several pathways of water molecule dissociation by electron have been reported [35]. These pathways reaction types included the momentum transfer, ionization, dissociative attachment, dissociative ionization, dissociation and dissociative excitation reactions. It has been reported that the rate of negative species produced by the dissociative attachment reactions (H^-, OH^- and O^-) was very small because their cross sections are weak ($1–6 \times 10^{-18}$ cm^2/molecule) [39].

The produced electron by the electron detachment would then participate in starting reaction with another water molecule and make a chain of reactions. This chain of reactions can be recombined by ion–ion or ion-molecular reaction.

In the current model, it was considered that the water vapor dissociation reactions pathway included OH^+, O^+ and H_2O^+ radicals. The chemical reactions list considered in this model are shown in Table 3. According to the literature survey, it is observed that the initiation of water vapor plasmolysis dissociation reaction with the previous radical as a reaction products is better than to start with the unlike reactions [39]. The simulation has been implemented using COMSOL Multiphysics plasma module and the electron collision cross sections as inputs import data [44].

Table 4 represents the surface reactions which are implemented in addition to the volumetric reactions.

The momentum transfer cross section can be determined by the following formula [26],

Table 3 Reaction mechanism of model II

Reaction	Reaction type	Type	Rate constant (K) [m^3/mol-sec, m^6/mol-sec]	References
1	$H_2O + e \rightarrow H_2O + e$	Momentum transfer reaction	3.65776E+11	[48]
2	$H_2O + e \rightarrow 2E + H_2O^+$	Ionization reaction	2.990E+05	[48]
3	$H_2O + e \rightarrow 2E + H + OH^+$	Dissociative ionization reaction	3.268E+02	[48]
4	$H_2O^+ + e \rightarrow H_2 + O$	Dissociative ion-recombination reaction	$f \times \left(0.3 \times 10^{-13}\left(0.01/T_e\right)\right)$	[48]
5	$H + OH^+ \rightarrow O^+ + H_2$	Charge transfer reaction	$f \times \left(4.9 \times 10^{-16} \exp^{(-0.36/T)}\right)$	[48, 49]

$f = 6.02 \times 10^{17}$; $g = 3.62404 \times 10^{35}$; T, gas temperature; T_e, electron temperature

Table 4 Surface reactions

Reaction	Reaction type	Sticking coefficient
1	$O^+ \rightarrow O$	1
2	$H_2O + O^+ \rightarrow H_2O^+ + O$	1

Table 5 The recommended momentum transfer cross section for E+H_2O [26]

Energy (eV)	Cross section (10^{-16} cm^2)
0.001861	430.3
0.005393	325
0.01563	228.4
0.04528	139.2
0.1312	60.71
0.3802	21.11
1.102	6.042
1.989	3.975
3.16	4.334
5.02	5.055
6.909	7.769
9.386	8.529
12.75	9.052
17.32	7.244
23.53	5.15
31.96	3.561
43.42	2.5
70	1.5
100	1

$$Q_m = 2\pi \int_0^{\pi} (1 - \cos\theta) q_{\text{elas}}(\theta) \sin\theta \, d\theta \tag{16}$$

where the elastic differential cross section is q_{elas}. The momentum transfer cross section can be determined by swarm experiments due to their low energies. Q_m can be obtained from the differential cross section (DCS) measured by the beam experiments. The momentum cross section data have been reported [50, 51]. The swarm values of momentum cross section almost show a good agreement with the beam data [50]. Finally, Table 5 presents the recommended momentum cross section data of electron collision with water.

The electron impact ionization cross sections of water vapor plasmolysis have been reviewed using the available experimental data [52–54]. The recommended values of the ionization cross section for H_2O are presented in Table 6.

It was seen that the cross section for OH^+ has a nonzero value at 17.5 eV, due to the uncertainty in the energy of the electron beam.

Reaction mechanism and cross section of Model III

Water vapor molecules are decomposed to their elements hydrogen and oxygen gas by the dissociation reaction using DBD plasma. In this model, the reaction mechanism that has been proposed by Fahad et al. [55] for water vapor decomposition using DBD plasma is simulated. Water vapor in this model is decomposed to combine O_2 and H_2 molecules after a chain of chemical reactions. Table 7 presents the reaction mechanism pathway.

In model III, we considered reactions (5) and (6) in Table 7 as the surface reactions. The reaction mechanism model presents that the water vapor is decomposed to form H, OH and H^-; then hydroxyl OH combines together to form H_2O_2. Water molecules and HO_2 are produced in reaction (4), then HO_2 reacts together to form H_2O_2 and O_2 molecules, and then HO_2 reacts with H to form hydrogen and oxygen molecules in reactions (5) and (6), respectively.

In this simulated reaction mechanism model, the water vapor molecules are decomposed to produce negative hydrogen (H^-) ions. Although the negative hydrogen ions have a weak cross sections because the dissociative attachment are very small, it is expected to generate a chain of chemical reactions. The recommended cross section of electron attachment of negative hydrogen ions is given in Table 8.

Analysis and simulation results

Simulation results of Model I

In this water vapor decomposition using DBD plasma simulation, the electron temperature, electric potential and the active species density are investigated. As explained in the previous section that model I presented the direct decomposition of water vapor using the DBD plasma to form hydrogen and oxygen molecules. Figure 4 shows the evolution of the electric potential at time zero and 0.225 s. It was clear the change of the electric potential between power and ground electrodes due to the positive charges aggregation on the dielectric covering the ground electrode.

The applied voltage evolutions across the applied plasma discharge gap with distance of (4.5 mm) are presented in Fig. 5 at different times. The electric field and electric potential between both electrodes are indicated in Fig. 6. It was seen that the electric field reaches to maximum in the gap between power and ground electrodes.

Table 6 The recommended ionization cross section for E+H_2O [26]

Energy (eV)	H_2O^+ (10^{-16} cm^2)	OH^+ (10^{-16} cm^2)	H^+ (10^{-16} cm^2)	H_2^+ (10^{-18} cm^2)	O^+ (10^{-18} cm^2)
13.5	0.025				
15	0.126				
17.5	0.272	0.0013			
20	0.411	0.0145	0.0024		
22.5	0.549	0.05	0.0091		
25	0.652	0.0855	0.0207		0.22
30	0.815	0.16	0.0433	0.018	0.37
35	0.958	0.222	0.0759	0.039	0.7
40	1.05	0.264	0.11	0.057	1.32
45	1.12	0.3	0.145	0.07	2.07
50	1.18	0.329	0.178	0.065	2.75
60	1.24	0.364	0.235	0.066	3.94
70	1.27	0.389	0.279	0.069	4.84
80	1.31	0.409	0.317	0.063	5.94
90	1.31	0.412	0.343	0.078	6.66
100	1.31	0.418	0.36	0.075	6.95
110	1.29	0.415	0.37	0.073	7.38
125	1.27	0.412	0.375	0.064	7.63
150	1.21	0.393	0.371	0.077	7.52
175	1.16	0.381	0.366	0.071	7.31
200	1.12	0.363	0.351	0.054	7.07
250	1.01	0.334	0.316	0.05	6.34
300	0.921	0.311	0.284	0.045	5.51
400	0.789	0.266	0.237	0.04	4.34
500	0.696	0.23	0.198	0.032	3.73
600	0.618	0.203	0.172	0.029	3.13
700	0.555	0.185	0.149	0.033	2.71
800	0.502	0.169	0.135	0.022	2.4
900	0.465	0.156	0.12	0.032	2.2
1000	0.432	0.143	0.109	0.024	1.94

Table 7 Reaction mechanism of model III

Reac.	Reaction type	Type	Rate constant (K) [m^3/mol-sec, m^6/mol-sec]	References
1	$H_2O + e \rightarrow H + OH + e$	Dissociation reaction	9.978E+07	[36, 48]
2	$H_2O + e \rightarrow H^- + OH$	Ionization reaction	3.706E+07	[42, 48]
3	$OH + OH \rightarrow H_2O_2$	Neutral–neutral reaction	1.02E+07	[36]
4	$OH + H_2O_2 \rightarrow H_2O + HO_2$	Neutral–neutral reaction	1.02E+06	[36]
5	$HO_2 + HO_2 \rightarrow H_2O_2 + O_2$	Surface reaction 1	9.64E+05	[36]
6	$HO_2 + H \rightarrow H_2 + O_2$	Surface reaction 2	3.91E+07	[36]

The hydrogen mass fraction and the electron density are shown in Fig. 7. In the first picture the hydrogen mass fraction is presented; it showed that the mass fraction increased over the time to reach the maximum value of 6.31×10^{-10}. It was observed that the electron density changed twice with the applied voltage positive and negative cycle; the maximum obtained electron density was 3.5×10^8 m^{-3}.

The electron density and electron temperature across the discharge gap at different times are shown in Figs. 8 and 9, respectively. It was observed that the electron density increased with time as well as in the electron temperature. Furthermore, the electron temperature and electron density reach to the maximum value inside the plasma discharge gap.

Table 8 The recommended cross section for H^- production from H_2O [26]

Energy (eV)	Cross section (10^{-18} cm^2)
5.5	0.02
5.74	0.16
5.9	0.985
6.01	4.3
6.1655	6.22
6.286	6.317
6.4	6.37
6.52	6.25
6.65	5.79
6.81	4.89
7	3.56
7.465	1.29
7.69	0.877
7.89	0.74
8	0.79
8.09	0.995
8.14	1.09
8.235	1.166
8.395	1.04
8.79	0.76
9.01	0.62
9.57	0.28
9.8	0.17
10	0.098

Simulation results of Model II

In this new proposed water vapor dissociation reaction mechanism simulation model II, the boundary conditions are same as model I, the reaction mechanisms pathway is more complicated than the first model, and the reaction mechanisms included H_2O^+, OH^+, and O^+ ions. It is considered in model II the unlike chemical reactions dissociation pathway explained in the previous section is excluded due to their low probability and high energy requirement [39]. Furthermore, it is expected that the hydrogen molecules produced from this mechanism will be higher than model I (direct water vapor decomposition). The results of the 1-D model II are analyzed by extruding the solution results in two dimensions. The surface plot has been investigated because it can represent how the variables evolve over time. Figure 10 presents the electric potential across the discharge gap over time. The plasma applied voltage is relatively changed in the positive and negative cycles between the power and ground electrode. The electric field and the electric potential are shown in Fig. 11 as a 2-D plot. It was clear from these pictures that the voltage is relatively uniform; it can more clearly be seen in the examining electric field. It was observed that the electric

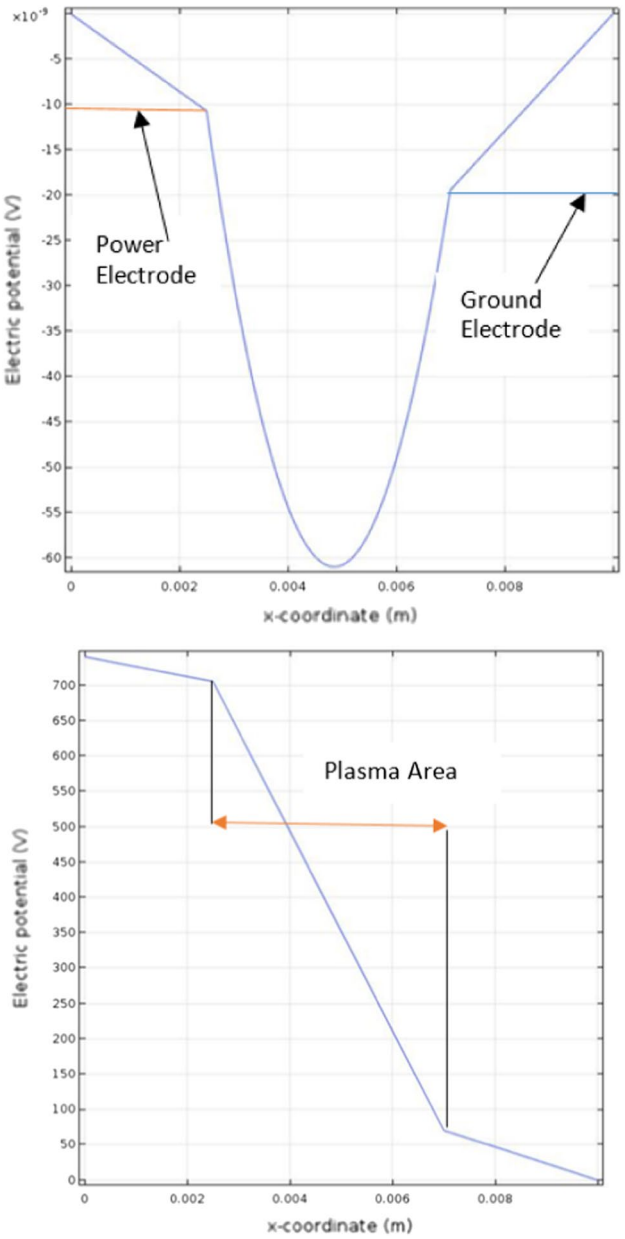

Fig. 4 Electric potential between both electrodes at 0 s and 0.225 s

field was much stronger in the plasma reaction area. The active species H_2 mass fraction and the electron density are indicated in Fig. 12. The hydrogen mass fraction was much higher than that obtained from the model I. Additionally, the excited species have a long lifetime in the plasma gap. The revolution of the electron density inside the gap also is presented in next picture.

The electron density and the electron temperature across the discharge gap are shown in Figs. 13 and 14, respectively. The electron temperatures are changed across the discharge gap over time to reach the maximum value of 180 V.

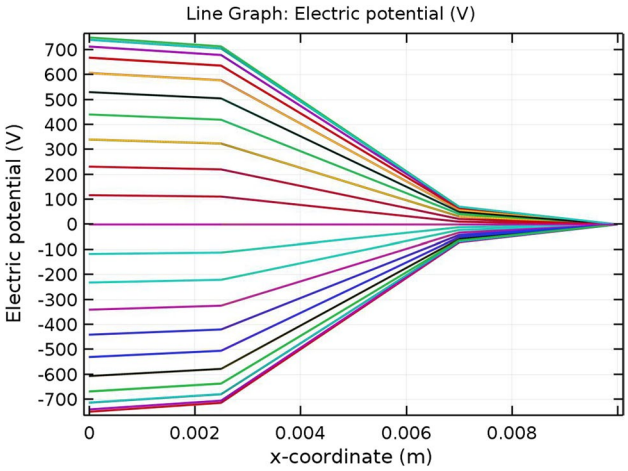

Fig. 5 The applied voltage at different times versus th discharge gap

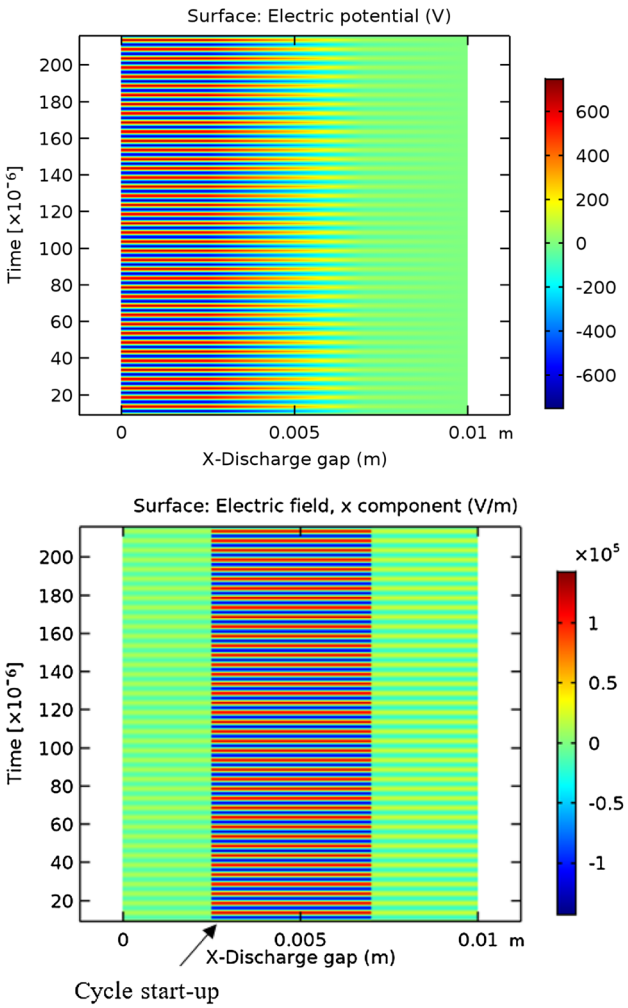

Fig. 6 The electric potential and the electric field versus the discharge gap

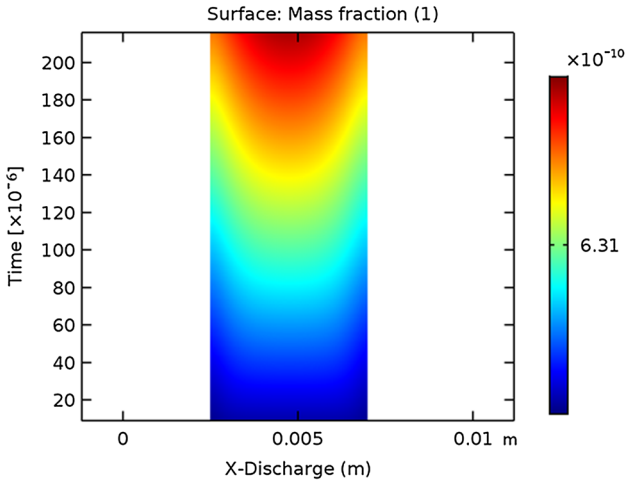

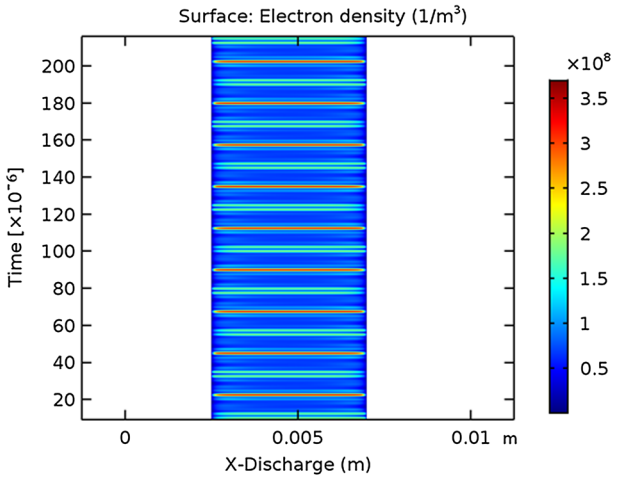

Fig. 7 The hydrogen mass fraction and the electron density versus the plasma discharge gap

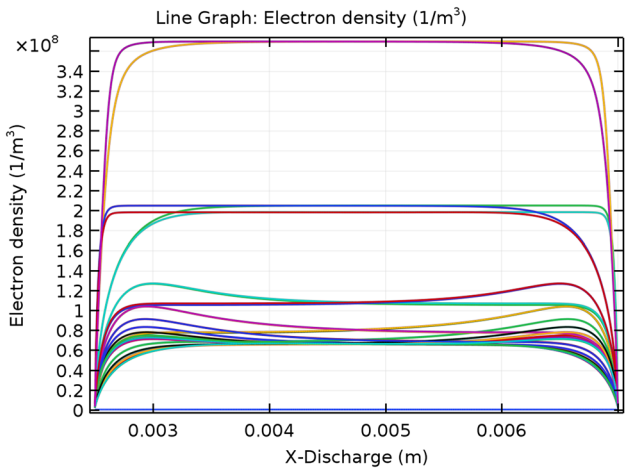

Fig. 8 The electron density versus the discharge gap

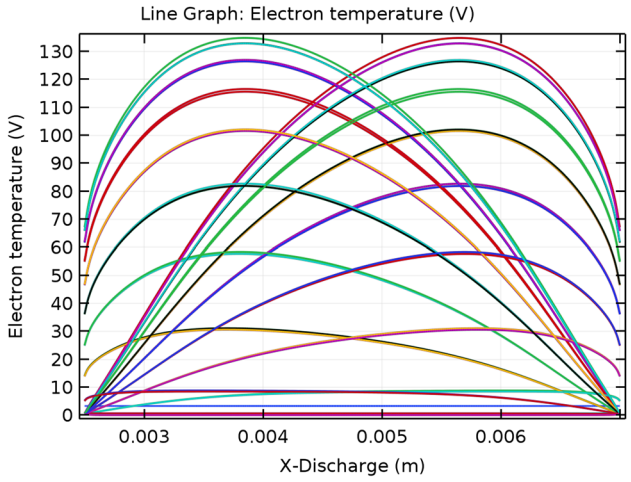

Fig. 9 The electron temperature versus the discharge gap

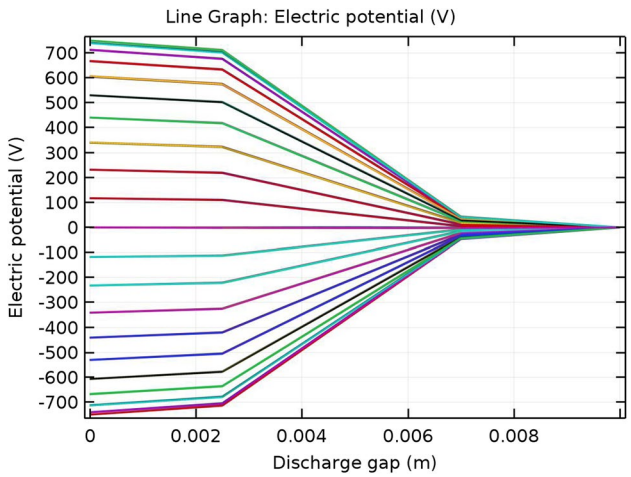

Fig. 10 The applied voltage over different times versus the discharge gap

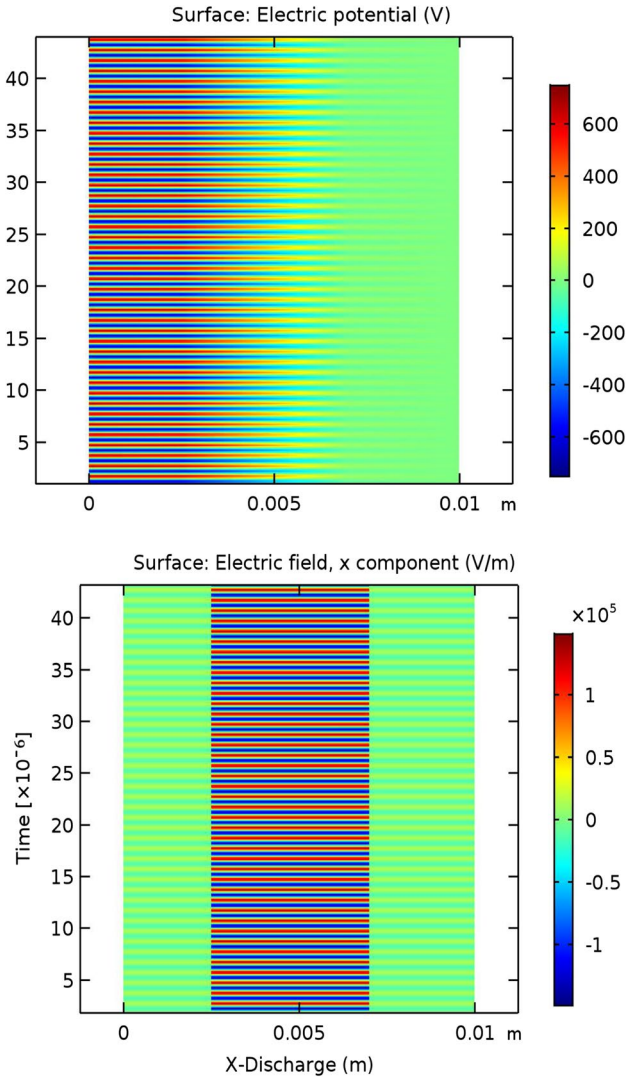

Fig. 11 The electric field and the electric potential versus the discharge gap

Simulation results of Model III

This model that simulates the water vapor plasmolysis reaction mechanisms has been proposed by Fahad et al. [55]. The water vapor molecules electrical breakdown are very complicated process; the dielectric plasma was formed inside the discharge gap at atmospheric pressure. The boundary conditions of this model are same as the previous models and the plasma is generated in the plasma gap (4.5 mm). This one-dimensional simulation is considered the first trail for water vapor decomposition using DBD plasma in the plate-type reactor. This model reaction mechanisms pathway includes negative hydrogen ions (H^-). The simulation results were implemented using a 2-D plot. Figure 15 shows the applied voltage change across the discharge distance in the negative and positive cycles.

Also, the applied voltage of model III is clearly seen uniform in the 2-D picture in Fig. 16. For more investigation of the effective area of the applied plasma, it can be seen in the electric field picture across the plasma discharge gap. In this model the electron collision cross section of H^- production from water vapor was utilized. The produced hydrogen molecules from the water vapor dissociation mechanism using DBD plasma in model III are presented in Fig. 17. It can be observed that the hydrogen produced from model III is much higher than that obtained from model I and model II. Furthermore, the produced hydrogen molecules mass fraction increased with the time to reach value of 1.64×10^{-7}. The electron density evolutions are depicted in the next picture of Fig. 17 versus the discharge gap distance. It was seen that the discharge cycle changed twice, one in the positive and the other in negative half cycle. The electron density

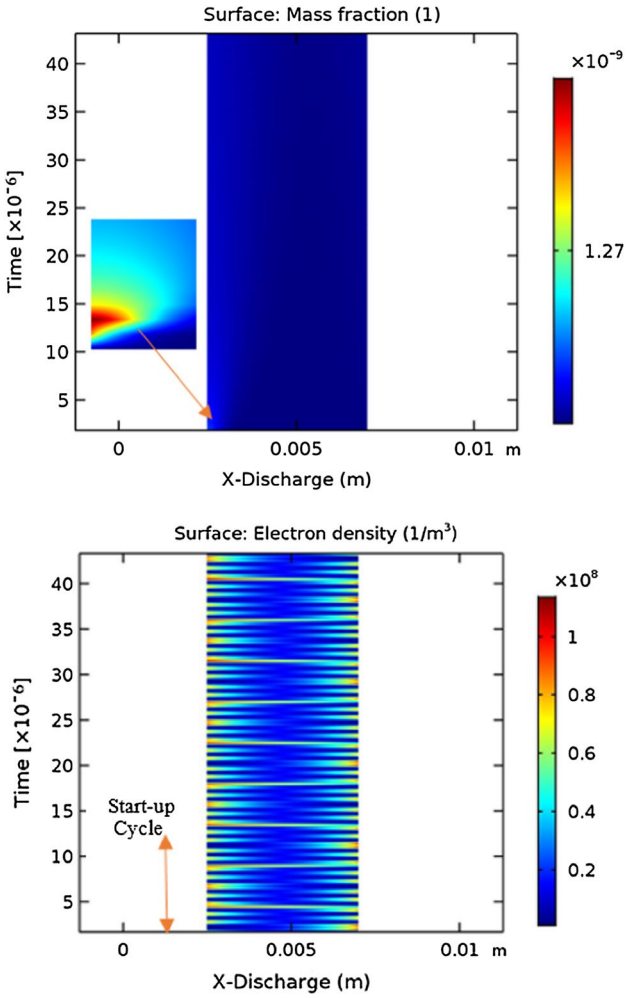

Fig. 12 Model II hydrogen mass fraction and the electron density versus the discharge gap

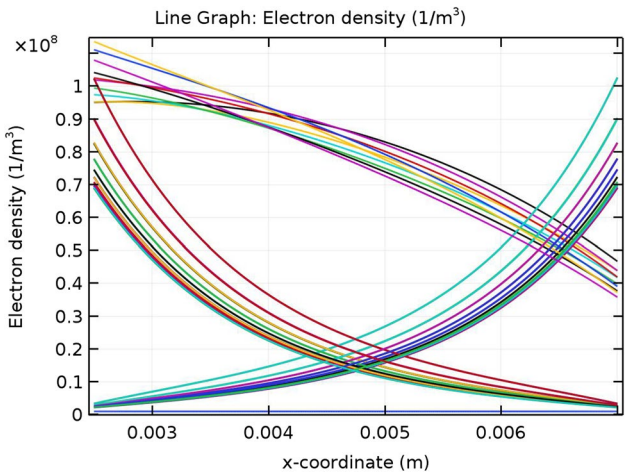

Fig. 13 The electron density versus the discharge gap

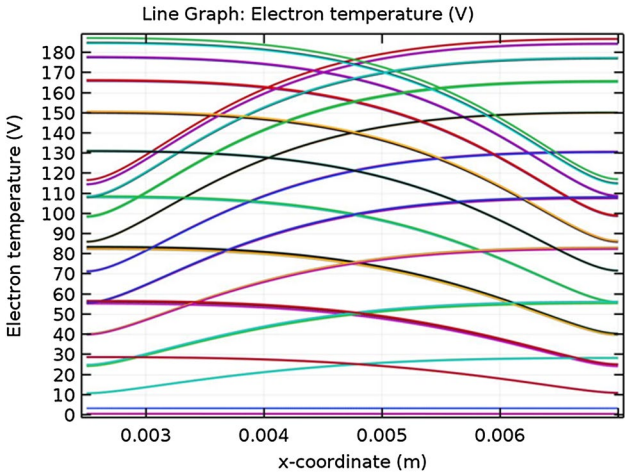

Fig. 14 The electron temperature versus the discharge gap

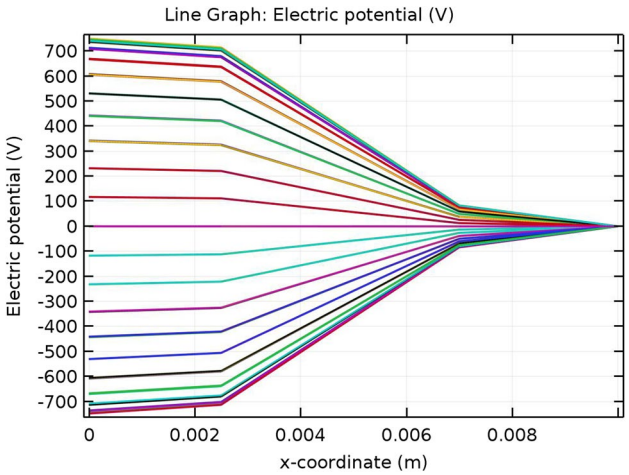

Fig. 15 Model III applied voltage over different times versus the discharge gap

and electron temperature change across the discharge gap distance are shown in Figs. 18 and 19, respectively. It was observed the maximum electron density values at the discharge gap center. The electron temperature revolution graph was clearly indicated the discharge cycles change over the time.

Comparison and discussions between models

A comparison between three models is shown in Fig. 20 for the produced hydrogen molecules mass fraction. For comparison the available data of three models log scale were used. It was clear that the model III hydrogen mass fraction was much higher than that obtained from model II and

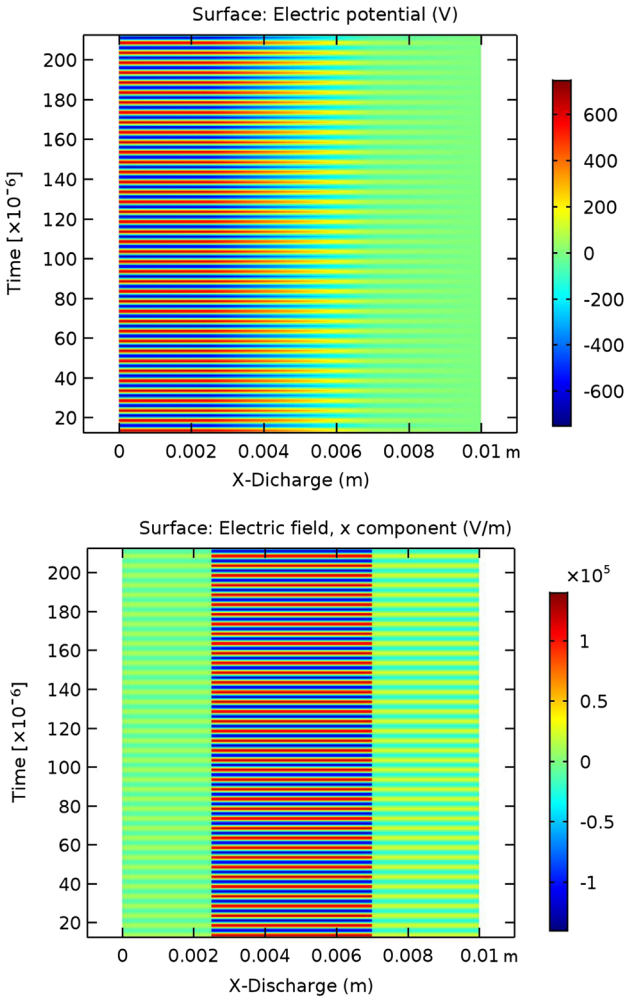

Fig. 16 Model III electric field and the electric potential versus the discharge gap

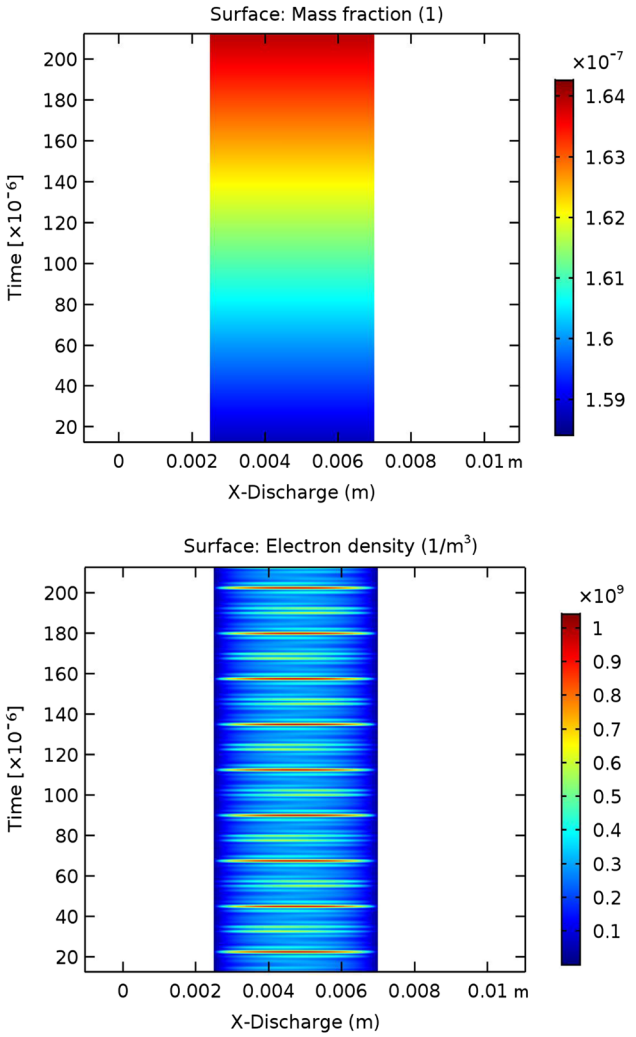

Fig. 17 Model II hydrogen mass fraction and the electron density versus the discharge gap

model I. Further, the hydrogen mass fraction of model II was higher than model I. It can be observed that the water vapor dissociation reaction mechanism pathway in the model III has much higher hydrogen production molecules. This simulation results have a good agreement with Fahad et al. [55] recommendation for water vapor decomposition reaction mechanisms pathway using DBD plasma.

Conclusion

Hydrogen production from water vapor using plasma has a great interest as a good solution for environmental issues. Further, the dielectric barrier discharge (DBD) is considered the simplest method to produce plasma at low gas temperature and atmospheric pressure. This simulation was carried out to study the DBD plasma characteristics and the densities of species using COMSOL Multiphysics package. Three

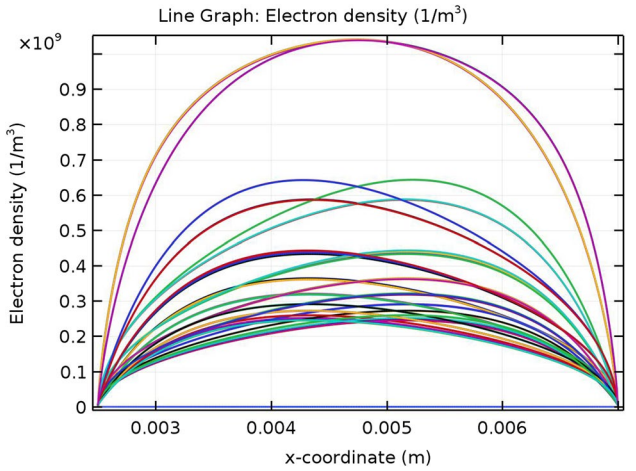

Fig. 18 The electron density versus the discharge gap

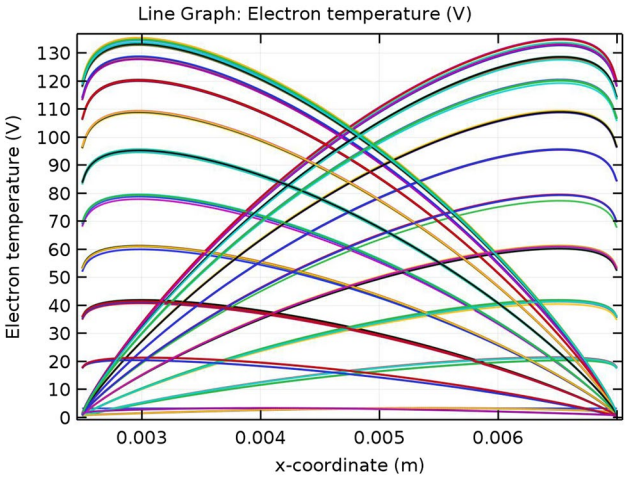

Fig. 19 The electron temperature versus the discharge gap

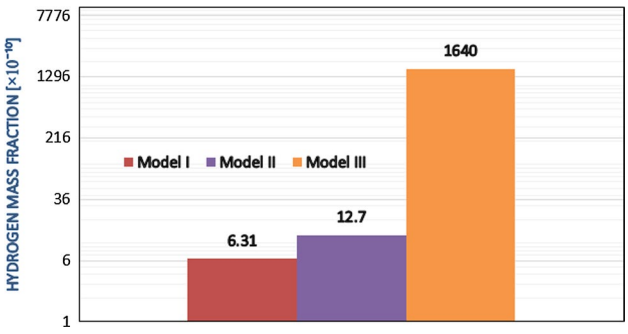

Fig. 20 Comparison between three models for H_2 mass fraction

models with different water vapor dissociation reaction mechanisms pathway were investigated. In the first model, the direct water vapor decomposition reaction was utilized; it was revealed that the hydrogen mass fraction increased across the plasma discharge gap over the time. More complicated reaction mechanism pathway in model II has been simulated included H_2O^+, OH^+, and O^+ ions; the electron collision cross sections have been prepared. It was observed that the produced H_2 molecules from model II were higher than model I. The electric potential and electric field across the discharge gap were simulated. It was found that the electric potential and electric field showed a significant changes inside the gap between the power and ground electrodes due to the charged species and plasma effect. The proposed and recommended water vapor plasmolysis dissociation model by Fahad et al. [55] has been simulated in model III. This model reaction mechanism pathway introduced H^- radical; the electron collision cross section of produced H^- from water vapor plasmolysis was utilized. It was seen that H^- radical controlled the H production by the electron detachment and H_2 was mainly produced from the reaction between HO_2 and H species. It was seen from the reaction kinetic modeling that H–H atom recombination wasn't the responsible for H_2 production. One of the most interesting simulation results was the growing of the H_2 mass fraction over time; additionally, it was found that the produced hydrogen molecules from model III were higher than model II and model I. The electron density and electron temperature evolution of these models were investigated across the plasma gap versus time. From the simulation results, it was clear that model III water vapor reaction mechanisms pathway was better than model II and model I.

Acknowledgments The author would like to thank **Prof.** Shinji Kambara for his continuous support for me and this project.

References

1. Chaubey, R., Sahu, S., James, O.O., Maity, S.: A review on development of industrial processes and emerging techniques for production of hydrogen from renewable and sustainable sources. Renew. Sustain. Energy Rev. **23**, 443–462 (2013)
2. Dincer, I.: Green methods for hydrogen production. Int. J. Hydrogen Energy **37**, 1954–1971 (2012)
3. Holladay, J.D., Hu, J., King, D.L., Wang, Y.: An overview of hydrogen production technologies. Catal. Today **139**, 244–260 (2009)
4. Freedom CAR & Fuel Partnership, Hydrogen Production Overview of Technology Options (2009)
5. El-Shafie, M., Kambara, S., Hayakawa, Y.: Hydrogen production technologies overview. J. Power Energy Eng. **7**, 107–154 (2019)
6. Yang, Xiao-Jun: A new integral transform operator for solving the heat-diffusion problem. Appl. Math. Lett. **64**, 193–197 (2017)
7. Zhang, Jian-Guo: The Fourier-Yang integral transform for solving the 1-D heat diffusion equation. Therm. Sci. **21**(1), S63–S69 (2017)
8. Yang, Xiao-Jun, GAO, F.: A new technology for solving diffusion and heat equations. Therm. Sci. **21**(1A), 133–140 (2017)
9. Yang, Xiao-Jun, Baleanu, Dumitru, Lazarevi, Mihailo P., Caji, Milan S.: Fractal boundary value problems for integral and differential equations with local fractional operators. Therm. Sci. **19**(3), 959–966 (2015)
10. Keidar, M., Beilis, I.: Plasma Engineering: Applications from Aerospace to Bio and Nanotechnology. Academic Press, Oxford (2013)
11. Sohbatzadeh, F., Colagar, A.H., Mirzanejhad, S., Mahmodi, S.: *E. coli*, *P. aeruginosa*, and *B. cereus* bacteria sterilization using afterglow of non-thermal plasma at atmospheric pressure. Appl. Biochem. Biotechnol. **160**, 1978–1984 (2010)
12. Sohbatzadeh, F., Mirzanejhad, S., Ghasemi, M., Talebzadeh, M.: Characterization of a non-thermal plasma torch in streamer mode and its effect on polyvinyl chloride and silicone rubber surfaces. J. Electrostat. **71**, 875–881 (2013)
13. Fridman, A.: Plasma Chemistry. Cambridge University Press, Cambridge (2008)
14. Fridman, G., Gutsol, A., Shekhter, A.B., Vasilets, V.N., Fridman, A.: Plasma processes. Polymer **5**(6), 503–533 (2008)
15. Roth, J.R.: Industrial Plasma Engineering: Volume 2—Applications to Nonthermal Plasma Processing. CRC Press, Boca Raton (2001)
16. El-Shafie, M., Kambara, S., Hayakawa, Y.: Preliminary results of hydrogen production from water vapor decomposition using DBD

plasma in a PMCR reactor. Int. J. Hydrogen Energy (2019). https://doi.org/10.1016/j.ijhydene.2019.05.199
17. Bockris, J.O.M., Dandapani, B., Cocke, D., Ghoroghchian, J.: On the splitting of water. Int. J. Hydrogen Energy **10**(3), 179–201 (1985)
18. Bernath, P.F.: For the spectroscopic observation of water. Phys. Chem. Chem. Phys. **4**, 1501 (2002)
19. Taylor, F.W.: The greenhouse effect and climate change revisited. Rep. Prog. Phys. **65**, 1 (2002)
20. Xie, X., Mumma, M.J.: The effect of electron collisions on rotational populations of cometary water. Astrophys. J. **386**, 720 (1992)
21. IAEA-TECDOC-799: Atomic and Molecular Data for Radiotherapy and Radiation Research. International Atomic Energy Agency, Vienna (1995)
22. Karwasz, G.P., Brusa, R.S., Zecca, A.: One century of experiments on electron-atom and molecule scattering: a critical review of integral cross-sections. Rivista Nuovo Cimento **24**(1), 146 (2001)
23. Shirai, T., Tabata, T., Tawara, H.: Analytic cross sections for electron collisions with CO, CO_2, and H_2O relevant to edge plasma impurities. At. Data Nucl. Data Tables **79**, 143 (2001)
24. Hayashi, M.: Bibliography of electron and photon cross sections with atoms and molecules. In: 20th Century–Water Vapour–NIFS-Data-81. National Institute for Fusion Science, Oroshi-cho, Toki, Japan (2003)
25. Itikawa, Y. (ed.): Photon and Electron Interactions with Atoms, Molecules and Ions, Landolt-Börnstein, vol. I/17, subvolume C. Springer, New York (2003)
26. Itikawa, Y., Mason, N.: Cross sections for electron collisions with water molecules. J. Phys. Chem. Ref. Data **34**(1), 1–22 (2005)
27. Gadkari, S., Tu, X., Gu, S.: Fluid model for a partially packed dielectric barrier discharge plasma reactor. Phys. Plasmas **24**, 093510 (2017)
28. Pan, J., Li, L., Chen, B., Song, Y., Zhao, Y., Xiu, X.: Numerical simulation of evolution features of the atmospheric-pressure CF4 plasma generated by the pulsed dielectric barrier discharge. Eur. Phys. J. D **70**, 136 (2016)
29. Abidat, R., Rebiai, S., Benterrouche, L.: Numerical simulation of atmospheric dielectric barrier discharge in helium gas using COMSOL Multiphysics. In: 2013 3rd International Conference on Systems and Control (ICSC), pp. 134–139. IEEE (2013)
30. Golubovskii, Y.B., Maiorov, V.A., Behnke, J., Behnke, J.F.: Modelling of the homogeneous barrier discharge in helium at atmospheric pressure. J. Phys. D **36**, 39 (2002)
31. Maehara, T., Toyota, H., Kuramoto, M., Iwamae, A., Tadokoro, A., Mukasa, S., et al.: Radio frequency plasma in water. Jpn. J. Appl. Phys. **45**(11), 8864–8868 (2006)
32. Burlica, R., Shih, K.Y., Locke, B.: Formation of H_2 and H_2O_2 in a water-spray gliding arc nonthermal plasma reactor. Ind. Eng. Chem. Res. **49**, 6342–6349 (2010)
33. Paulmier, T., Fulcheri, L.: Use of non-thermal plasma for hydrocarbon reforming. Chem. Eng. J. **106**(1), 59–71 (2005)
34. Mededovic, S., Finney, W.C., Locke, B.R.: Electrical discharges in mixtures of light and heavy water. Plasma Process. Polym. **5**(1), 76–83 (2008)
35. Avtaeva, S., General, A., Kel'man, V.: Kinetic model for low density non-stationary gas discharge in water vapour. J. Phys. D Appl. Phys. **43**, 315201 (2010)
36. Sobacchi, M., Saveliev, A., Fridman, A., Kennedy, L.A., Ahmed, S., Krause, T.: Experimental assessment of a combined plasma/catalytic system for hydrogen production via partial oxidation of hydrocarbon fuels. Int. J. Hydrogen Energy **27**(6), 635–642 (2002)
37. Lias, S.G.: Ionization energy evaluation. In: P.J. Linstrom and W.G. Mallard (eds.) NIST Chemistry WebBook. NIST Standard Reference Database Number 69. National Institute of Standards and Technology, Gaithersburg, MD. http://webbook.nist.gov (2001)
38. Ruscic, B., et al.: On the enthalpy of formation of hydroxyl radical and gas-phase bond dissociation energies of water and hydroxyl. J. Phys. Chem. A **106**, 2727 (2002)
39. Dolan, T.: Electron and ion collisions with water vapour. J. Phys. D Appl. Phys. **26**, 4 (1993)
40. Lozano-Parada, J.H., Zimmerman, W.B.: The role of kinetics in the design of plasma microreactors. Chem. Eng. Sci. **65**(17), 4925–4930 (2010)
41. Lias, S.G.: Ionization energy evaluation. In: Linstrom, P.J., Mallard, W.G. (eds.) NIST Chemistry WebBook, NIST Standard Reference Database Number 69. National Institute of Standards and Technology, Gaithersburg, MD. http://webbook.nist.gov. (2001)
42. Šingliar, M.: Solar energy using for hydrogen production. Pet. Coal **49**(2), 40–47 (2007)
43. Lieberman, M.A., Lichtenberg, A.J.: Principles of Plasma Discharges and Materials Processing. Wiley, Hoboken (2005)
44. Zimmerman, W.B.J.: Multiphysics Modeling with Finite Element Methods, Series on Stability, Vibration and Control of Systems, Series A, vol. 18. World Scientific Publishing Company, London (2006)
45. Schutten, J., de Heer, F.J., Moustafa, H.R., Boerboom, A.J.H., Kistemaker, J.: Gross- and partial-ionization cross sections for electrons on water vapor in the energy range 0.1–20 keV. J. Chem. Phys. **44**(10), 3924–3928 (1966)
46. Lukes, P., Clupek, M., Babicky, V., Simek, M., Tothova, I., Janda, V., et al.: Role of solution conductivity in the electron impact dissociation of H_2O induced by plasma processes in the pulsed corona discharge in water. In: HAKONE XI, 11th International Symposium on High Pressure, Low Temperature Plasma Chemistry, Contributed Papers, Oleron Island (2008)
47. Locke, B., Sato, M., Sunka, P., Hoffmann, M., Chang, J.S.: Electrohydraulic discharge and nonthermal plasma for water treatment. Ind. Eng. Chem. Res. **45**(3), 882–905 (2006)
48. Jasinski, M., Dors, M., Mizeraczyk, J.: Production of hydrogen via methane reforming using atmospheric pressure microwave plasma. J. Power Sources **181**(1), 41–45 (2008)
49. Shih, K.Y., Locke, B.R.: Optical and electrical diagnostics of the effects of conductivity on liquid phase electrical discharge. IEEE Trans. Plasma Sci. **99**, 1–10 (2010)
50. Cho, H., Park, Y.S., Tanaka, H., Buckman, S.J.: Measurements of elastic electron scattering by water vapour extended to backward angles. J. Phys. B At. Mol. Opt. Phys. **37**, 625–634 (2004)
51. Yousfi, M., Benabdessadok, M.D.: Boltzmann equation analysis of electron-molecule collision cross sections in water vapor and ammonia. J. Appl. Phys. **80**, 6619–6630 (1996)
52. Lindsay, B.G., Mangan, M.A.: In: Itikawa, Y. (ed.) Photon and Electron Interactions with Atoms, Molecules and Ions, Landolt-Börnstein, vol. I/17, subvolume C. Springer, New York (2003)
53. Straub, H.C., Lindsay, B.G., Smith, K.A., Stebbings, R.F.: Absolute partial cross sections for electron-impact ionization of H_2O and D_2O from threshold to 1000 eV. J. Chem. Phys. **108**, 109–116 (1998)
54. Rao, M.V.V.S., Iga, I., Srivastava, S.K.: Ionization cross-sections for the production of positive ions from H: O by electron impact. J. Geophys. Res. **100**, 421–425 (1995)
55. Rehman, F., Lozano-Parada, J.H., Zimmerman, W.B.: A kinetic model for H_2 production by plasmolysis of water vapours at atmospheric pressure in a dielectric barrier discharge microchannel reactor. Int. J. Hydrogen Energy **37**, 17678–17690 (2012)